Supplemental Materials - Methods

Methods Section 1 - remote sensing methods for wetland hydrology trends

Following the methods that Donnelly et al. (2021) outlined, wetland and agricultural surface water conditions were measured monthly as a five-year running means using constrained spectral mixture analysis (SMA; Adams and Gillespie, 2006). This approach allowed proportional estimations of water contained within a continuous 30×30 m pixel grid (Halabisky et al., 2016; Jin et al. 2017) and provided an accurate account of flooding when detectability was reduced due to interspersion of emergent vegetation, shallow, or turbid water (DeVries et al., 2017), characteristics common to seasonal wetlands in semi-arid regions (Jolly et al., 2008). Because these conditions can partially mask areas covered with water (Donnelly et al., 2019), we considered pixels fully inundated when water was present. Pixels containing <15% surface water were omitted from summaries to minimize the overestimation of surface water area.

Satellite data used for SMA were formatted by binning individual Landsat scenes by month and averaging results into twelve composite images for each five-year mean. Results provided 444 unique monthly measures of wetland-agriculture surface water for the SONEC and Central Valley regions. Areas containing cloud, cloud shadow, snow, and ice were masked using the Landsat CFMask band (Foga et al., 2017). All unmasked pixels in Landsat 30 m visible, near-infrared, and short wave infrared bands were incorporated into SMA except for Landsat 8 coastal aerosol band. Surface water was not measured in 2012 due to poor quality satellite imagery.

Training data for SMA were extracted from satellite imagery as spectral end members unique to individual images classified. Training site locations represented homogeneous land cover types mapped as water, wetland vegetation, upland, and alkali soil. Spectral end members for water were collected using image masks generated from 99th percentile normalized difference water index values (McFeeters, 1996), coincident with large deepwater lakes within both regions. A similar masking approach was applied to collect wetland vegetation end members using normalized difference vegetation indices (Box et al., 1989). Sampling was constrained to sites coincident with flooded wetlands and representative of associated plant phenology. Spectral mixture analysis requires minimal training data (Adams and Gillespie, 2006) that allows upland and alkali soil end members to be generated from a small number of static plots within the regions (n = 4; 0.5-1 km^2). Upland plots were associated with homogenous shrublands characterized by low vegetative productivity and high soil exposure. Alkali soil plots were coincident with dry lake basins in surface mineral deposits. Plot locations were identified using high resolution (< 0.5 m) multispectral satellite imagery or field survey. All image processing and raster‐based analyses were conducted using Google Earth Engine cloud‐based geospatial processing platform (Gorelick et al., 2017).

Supplemental Section 2 - change detection methods for wetland loss

Change detection analysis was used to designate wetland or flooded agricultural declines as functional or physical loss to discern underlying drivers of change. Functional losses were attributed to areas of diminishing surface water (i.e. drying) associated with shifts in ecological water balance or water management in the absence of physical alterations. Land conversion (e.g., urban expansion or shifting agricultural practices) resulting in surface water declines were identified as physical loss. Areas of change were delineated by differencing mean monthly (Jan-Dec) surface water conditions between P1 (1984-1991) and P2 (2013-20). Using a GIS, change areas were visually inspected through on-screen photo-interpretation of high resolution (≤ 1 m) multispectral satellite imagery (acquired 2018 or later) to identify areas of physical loss. Surface water conditions for P1 and P2 were derived using remote-sensing methods outlined in Supplemental Section 1. All image processing and raster-based analyses were conducted using Google Earth Engine cloud-based geospatial processing platform (Gorelick et al., 2017). GIS analyses were performed using QGIS (QGIS Development Team, 2020).

Supplemental Section 3 - eBird-traditional survey comparison

To compare temporal abundance distributions derived from the eBird Basic Dataset (EBD) (Sullivan et al., 2009) and traditional survey methods (i.e., aerial survey and systematic ground counts), waterbird counts were binned bi-weekly and summed across years. Results were then grouped by region, species, and survey type and scaled to relative values. Boxplots and non-parametric Wilcoxon tests were used to display and compare data graphically. All available EBD observations collected from 1984 to 2020 in the SONEC and Central Valley regions were used in our evaluation. SONEC bi-weekly aerial waterfowl surveys conducted in the Klamath Basin from 1984-2016 were used for EBD evaluation. Because surveys were flown during spring (Jan-May) and fall (Sep-Dec), distributions were compared for each period using four migrating dabbling duck species (Fig. S1-2). Although aerial survey efforts were conducted for a subset of SONEC, results were considered representative of regional waterfowl use patterns (Donnelly et al., 2019).

Bi-weekly ground surveys on the Sacramento National Wildlife Refuge Complex (hereafter ‘refuge complex’) were used in the Central Valley for EBD evaluation. Ground surveys were collected from 2011 to 2017 across six independent refuge units representing the northern half of the Central Valley study area. For comparison, we selected five wintering waterfowl (Figs. S3) and three fall migrating shorebird species (Fig. S4) based on their use of habitats associated with the refuge complex. SONEC and Central Valley comparisons showed no significant differences in temporal abundance patterns. Outcomes support previous results from Callaghan and Gawlik (2015) and Walker and Taylor (2017) that showed EBD observations and traditional survey efforts equivalent when applied at broad scales.

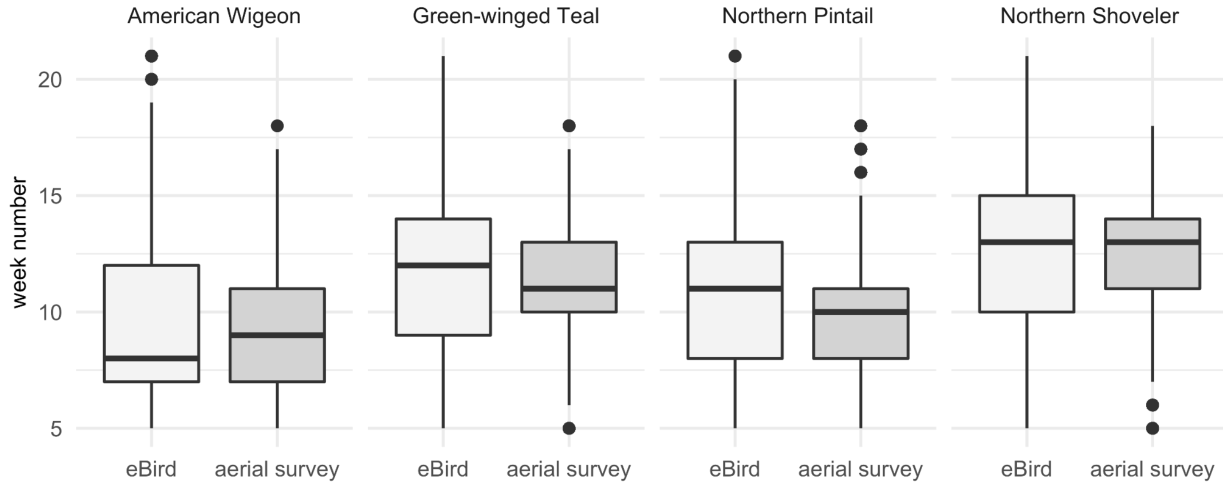

Figure S1**.** Temporal distribution of dabbling duck abundance derived from eBird Basic Dataset and aerial surveys collected during spring migration (Feb-May) in SONEC. Distributions representative of all available eBird (1984-2020) and aerial survey counts (1984 to 2016). Nonparametric Wilcoxon tests results by species: American Wigeon p-value 0.258, Green-winged Teal p-value 0.776, Northern Pintail p-value 0.315, Northern Shoveler p-value 0.972. Boxes, interquartile range (IQR); line dividing the box horizontally, median value; whiskers, 1.5 times the IQR; points, outliers.

temporal distribution of dabbling duck abundance derived from

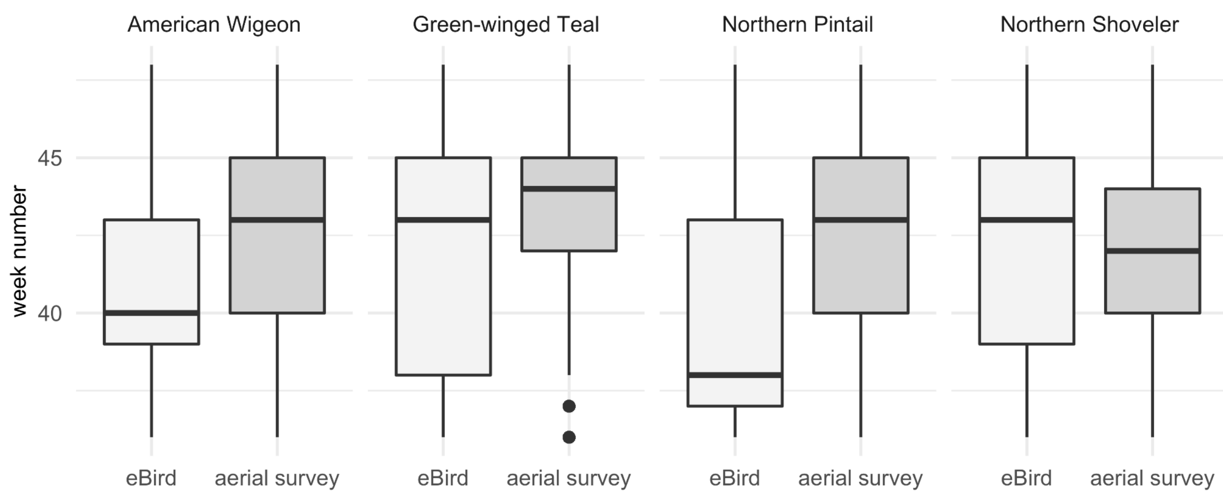

Figure S2.Temporal distribution of dabbling duck abundance derived from eBird Basic Dataset and aerial surveys collected during spring migration (Sep-Dec) in SONEC. Distributions representative of all available eBird (1984-2020) and aerial survey counts (1984 to 2016). Nonparametric Wilcoxon tests results by species: American Wigeon p-value 0.258, Green-winged Teal p-value 0.776, Northern Pintail p-value 0.315, Northern Shoveler p-value 0.972. Boxes, interquartile range (IQR); line dividing the box horizontally, median value; whiskers, 1.5 times the IQR; points, outliers.

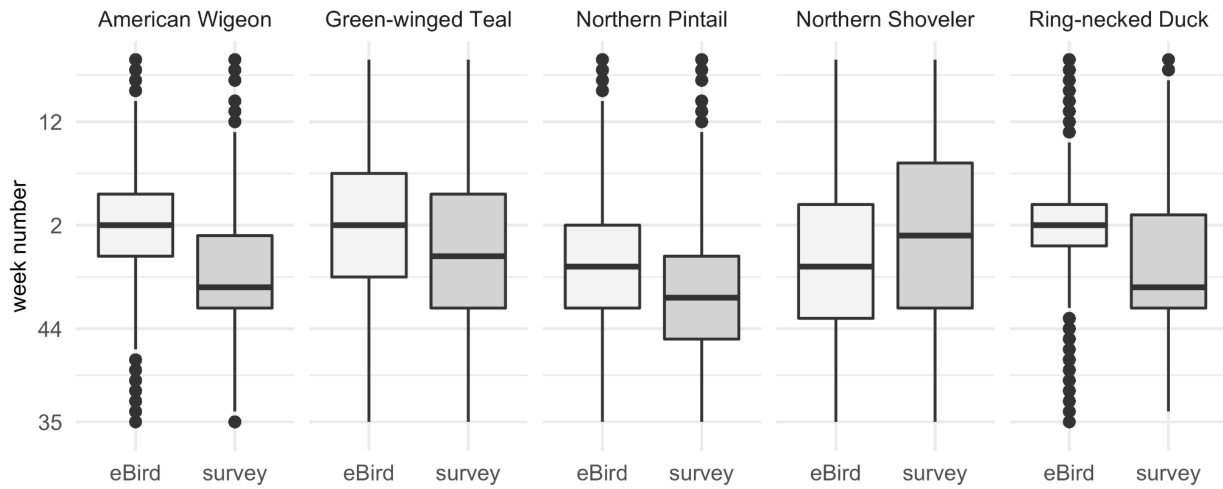

Figure S3. Temporal distribution of dabbling duck abundance derived from eBird Basic Dataset and ground surveys collected during the wintering period (Oct-Mar) in the Central Valley. Distributions representative of all available eBird (1984-2020) and ground survey counts (2011 to 2017). Nonparametric Wilcoxon tests results by species: American Wigeon p-value 0.480, Green-winged Teal p-value 0.893, Northern Pintail p-value 0.757, Northern Shoveler p-value 0.941, Ring-necked Duck p-value 0.628. Boxes, interquartile range (IQR); line dividing the box horizontally, median value; whiskers, 1.5 times the IQR; points, outliers.

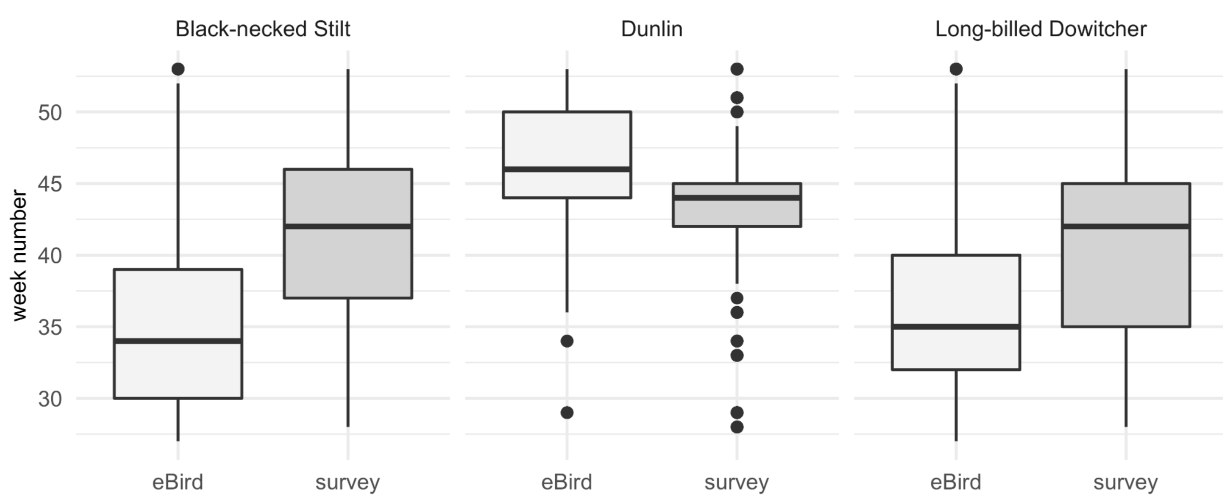

Figure S4. Temporal distribution of shorebird abundance derived from eBird Basic Dataset and ground surveys collected from August to December in the Central Valley (see Fig. 1). Distributions representative of all available eBird (1984-2020) and ground survey counts (2011 to 2017). Nonparametric Wilcoxon tests results by species: Black-necked Stilt p-value 0.968, Dunlin p-value 0.072, Long-billed Dowitcher p-value 0.698. Boxes, interquartile range (IQR); line dividing the box horizontally, median value; whiskers, 1.5 times the IQR; points, outliers.

Supplementary Materials -- Results

Table S1. SONEC all wetlands - P1 (1988-2004) and P2 (2005-20) median monthly surface water change. Areas (ha) include wetlands associated with closed basin lakes, public-private lands, and wildlife refuges.

Hydroperiod	Month	P1 (1988-2004)	P2 (2004-2020)	Difference	% Difference	Wilcox *p*
semi-permanent	Jan	183,964	89,818	-94,147	-51%	0.000
	Feb	189,984	122,833	-67,151	-35%	0.002
	Mar	213,765	156,377	-57,388	-27%	0.000
	Apr	220,250	160,551	-59,699	-27%	0.000
	May	246,637	157,925	-88,712	-36%	0.000
	Jun	242,978	162,556	-80,422	-33%	0.000
	Jul	243,206	152,021	-91,185	-37%	0.000
	Aug	229,178	144,744	-84,434	-37%	0.000
	Sep	216,979	140,497	-76,482	-35%	0.000
	Oct	216,636	117,410	-99,226	-46%	0.000
	Nov	194,011	113,630	-80,381	-41%	0.000
	Dec	187,751	110,171	-77,580	-41%	0.000
seasonal	Jan	22,687	18,139	-4,547	-20%	0.102
	Feb	36,228	39,209	2,980	8%	0.204
	Mar	41,984	50,821	8,836	21%	0.004
	Apr	39,804	52,155	12,351	31%	0.001
	May	37,862	51,196	13,334	35%	0.002
	Jun	33,661	45,951	12,290	37%	0.001
	Jul	22,837	16,408	-6,429	-28%	0.023
	Aug	5,562	3,845	-1,717	-31%	0.191
	Sep	2,849	2,993	144	5%	0.998
	Oct	4,651	7,428	2,778	60%	0.001
	Nov	10,793	12,104	1,312	12%	0.049
	Dec	18,119	18,716	598	3%	0.873
temporary	Jan	27,519	40,603	13,084	48%	0.136
	Feb	56,432	55,041	-1,390	-3%	0.606
	Mar	37,641	39,312	1,671	4%	0.709
	Apr	23,915	32,674	8,759	37%	0.191
	May	19,081	31,081	12,000	63%	0.000
	Jun	13,315	15,191	1,876	14%	0.204
	Jul	3,986	2,054	-1,932	-49%	0.008
	Aug	388	605	217	56%	0.127
	Sep	385	509	123	32%	0.045
	Oct	987	2,028	1,041	106%	0.000
	Nov	9,116	9,372	256	3%	0.465
	Dec	24,954	23,567	-1,387	-6%	0.444

Table S2. SONEC closed basin lakes - P1 (1988-2004) and P2 (2005-20) median monthly surface water change. Areas (ha) inclusive of all littoral-lacustrine wetland systems.

Hydroperiod	Month	P1 (1988-2004)	P2 (2004-2020)	Difference	% Difference	Wilcox *p*
semi-permanent	Jan	132,014	62,045	-69,969	-53%	0.000
	Feb	147,516	88,625	-58,891	-40%	0.001
	Mar	157,163	113,450	-43,712	-28%	0.000
	Apr	167,473	115,991	-51,481	-31%	0.000
	May	183,108	120,152	-62,956	-34%	0.000
	Jun	182,999	122,005	-60,994	-33%	0.000
	Jul	182,902	117,643	-65,259	-36%	0.000
	Aug	178,617	114,286	-64,331	-36%	0.000
	Sep	169,799	112,115	-57,685	-34%	0.000
	Oct	167,106	88,037	-79,069	-47%	0.000
	Nov	151,571	84,091	-67,481	-45%	0.000
	Dec	145,878	85,281	-60,597	-42%	0.000
seasonal	Jan	4,298	6,733	2,434	57%	0.326
	Feb	8,231	11,888	3,657	44%	0.025
	Mar	6,499	17,371	10,872	167%	0.005
	Apr	9,385	23,608	14,223	152%	0.000
	May	11,409	24,169	12,760	112%	0.000
	Jun	10,476	22,618	12,142	116%	0.000
	Jul	8,661	8,502	-159	-2%	0.845
	Aug	2,099	2,240	141	7%	0.763
	Sep	864	1,621	757	88%	0.245
	Oct	1,120	2,574	1,454	130%	0.001
	Nov	2,322	5,976	3,654	157%	0.000
	Dec	4,569	7,818	3,250	71%	0.058
temporary	Jan	4,798	8,324	3,526	74%	0.025
	Feb	7,649	12,314	4,664	61%	0.045
	Mar	2,675	7,363	4,688	175%	0.023
	Apr	3,647	12,830	9,183	252%	0.001
	May	3,699	13,504	9,806	265%	0.000
	Jun	2,041	7,504	5,463	268%	0.001
	Jul	1,122	498	-624	-56%	0.245
	Aug	87	264	177	203%	0.017
	Sep	93	205	111	119%	0.003
	Oct	159	563	404	254%	0.000
	Nov	855	1,944	1,089	127%	0.009
	Dec	4,420	4,793	373	8%	0.736

Table S3. SONEC wildlife refuges - P1 (1988-2004) and P2 (2005-20) median monthly surface water change. Areas (ha) exclusive to state and federally managed wildlife refuges.

Hydroperiod	Month	P1 (1988-2004)	P2 (2004-2020)	Difference	% Difference	Wilcox *p*
semi-permanent	Jan	12,870	8,714	-4,156	-32%	0.000
	Feb	15,623	11,399	-4,224	-27%	0.000
	Mar	15,566	12,578	-2,989	-19%	0.000
	Apr	14,658	12,449	-2,209	-15%	0.001
	May	15,107	11,128	-3,979	-26%	0.000
	Jun	14,756	11,296	-3,460	-23%	0.000
	Jul	13,063	9,765	-3,298	-25%	0.000
	Aug	11,691	8,262	-3,429	-29%	0.000
	Sep	11,348	7,803	-3,544	-31%	0.000
	Oct	12,695	10,401	-2,295	-18%	0.000
	Nov	13,898	10,884	-3,015	-22%	0.000
	Dec	12,810	9,613	-3,197	-25%	0.000
seasonal	Jan	6,466	4,054	-2,412	-37%	0.031
	Feb	11,319	7,059	-4,260	-38%	0.204
	Mar	11,844	13,278	1,434	12%	0.309
	Apr	9,202	10,816	1,614	18%	0.127
	May	5,709	7,595	1,886	33%	0.034
	Jun	3,962	6,613	2,651	67%	0.015
	Jul	1,836	1,887	51	3%	0.873
	Aug	360	304	-56	-16%	0.533
	Sep	378	335	-42	-11%	0.231
	Oct	1,059	1,179	119	11%	0.292
	Nov	3,093	2,243	-850	-27%	0.017
	Dec	4,967	3,797	-1,170	-24%	0.023
temporary	Jan	6,364	4,771	-1,593	-25%	0.790
	Feb	13,003	8,342	-4,660	-36%	0.005
	Mar	10,580	9,657	-923	-9%	0.292
	Apr	5,986	4,498	-1,488	-25%	0.488
	May	2,393	2,490	98	4%	0.709
	Jun	1,186	1,997	812	68%	0.025
	Jul	574	410	-164	-29%	0.191
	Aug	55	93	38	68%	0.008
	Sep	94	112	18	20%	0.557
	Oct	280	353	72	26%	0.402
	Nov	1,362	1,142	-220	-16%	0.276
	Dec	5,264	3,740	-1,524	-29%	0.146

Table S4. SONEC public wetlands - P1 (1988-2004) and P2 (2005-20) median monthly surface water change. Areas (ha) encompass un-managed or natural wetlands on public lands administered by, but not limited to the U.S. Forest Service and Bureau of Land Management.

Hydroperiod	Month	P1 (1988-2004)	P2 (2004-2020)	Difference	% Difference	Wilcox *p*
	Jan	13,525	5,361	-8,164	-60%	0.008
	Feb	12,800	10,234	-2,566	-20%	0.041
	Mar	18,875	11,332	-7,543	-40%	0.000
	Apr	16,487	11,763	-4,724	-29%	0.002
	May	18,244	11,030	-7,214	-40%	0.000
semi-permanent	Jun	17,704	11,381	-6,323	-36%	0.000
	Jul	17,971	10,184	-7,787	-43%	0.000
	Aug	16,598	9,537	-7,061	-43%	0.001
	Sep	13,358	9,085	-4,273	-32%	0.000
	Oct	13,338	9,078	-4,260	-32%	0.003
	Nov	13,564	9,434	-4,131	-30%	0.000
	Dec	12,245	6,278	-5,967	-49%	0.004
	Jan	4,785	2,501	-2,284	-48%	0.034
	Feb	7,265	9,342	2,077	29%	0.023
	Mar	9,660	10,191	531	6%	0.790
	Apr	9,884	10,491	607	6%	0.873
	May	11,063	8,999	-2,064	-19%	0.074
seasonal	Jun	9,880	8,284	-1,596	-16%	0.034
	Jul	7,611	2,811	-4,800	-63%	0.000
	Aug	1,591	846	-745	-47%	0.002
	Sep	783	568	-215	-27%	0.231
	Oct	767	1,149	382	50%	0.037
	Nov	2,161	2,612	452	21%	0.231
	Dec	3,267	3,230	-37	-1%	0.817
	Jan	5,234	7,199	1,965	38%	0.326
	Feb	12,039	14,409	2,370	20%	0.260
	Mar	8,669	7,578	-1,091	-13%	0.292
	Apr	5,497	6,774	1,277	23%	0.292
	May	4,987	5,849	863	17%	0.709
temporary	Jun	3,961	3,353	-608	-15%	0.309
	Jul	864	310	-554	-64%	0.000
	Aug	68	101	32	47%	0.631
	Sep	63	58	-4	-7%	0.986
	Oct	100	336	236	237%	0.000
	Nov	1,791	2,863	1,073	60%	0.010
	Dec	5,398	6,972	1,574	29%	0.736

Table S5. SONEC private wetlands - P1 (1988-2004) and P2 (2005-20) median monthly surface water change. Areas (ha) exclusive to private un-managed or natural wetlands.

Hydroperiod	Month	P1 (1988-2004)	P2 (2004-2020)	Difference	% Difference	Wilcox *p*
semi-permanent	Jan	8,322	6,285	-2,037	-24%	0.110
	Feb	9,699	9,029	-670	-7%	0.245
	Mar	12,909	11,154	-1,755	-14%	0.045
	Apr	12,761	11,157	-1,605	-13%	0.157
	May	12,691	9,564	-3,127	-25%	0.045
	Jun	12,705	10,767	-1,937	-15%	0.058
	Jul	12,502	9,748	-2,754	-22%	0.015
	Aug	11,351	7,978	-3,373	-30%	0.037
	Sep	9,676	7,006	-2,670	-28%	0.058
	Oct	10,644	6,959	-3,684	-35%	0.045
	Nov	10,236	7,343	-2,893	-28%	0.004
	Dec	9,232	5,210	-4,022	-44%	0.008
seasonal	Jan	5,046	3,315	-1,731	-34%	0.510
	Feb	9,102	8,856	-246	-3%	0.657
	Mar	9,819	11,080	1,261	13%	0.136
	Apr	8,504	9,984	1,480	17%	0.276
	May	8,726	8,768	42	1%	0.901
	Jun	7,699	8,311	612	8%	0.488
	Jul	4,862	3,316	-1,546	-32%	0.000
	Aug	1,279	672	-607	-48%	0.009
	Sep	588	428	-159	-27%	0.292
	Oct	687	891	204	30%	0.382
	Nov	2,527	1,889	-638	-25%	0.087
	Dec	3,154	2,507	-647	-21%	0.709
temporary	Jan	7,144	7,119	-25	0%	0.606
	Feb	16,040	16,950	910	6%	0.292
	Mar	10,098	9,812	-286	-3%	0.929
	Apr	5,325	5,543	218	4%	0.790
	May	3,537	3,281	-256	-7%	0.986
	Jun	2,679	2,682	3	0%	0.817
	Jul	984	487	-496	-50%	0.010
	Aug	115	94	-21	-18%	0.606
	Sep	74	89	15	21%	0.444
	Oct	158	222	64	41%	0.028
	Nov	2,403	2,069	-334	-14%	0.191
	Dec	5,970	6,382	412	7%	0.958

Table S6. SONEC flooded agriculture - P1 (1988-2004) and P2 (2005-20) median monthly surface water change. Grass hay cultivation accounted for the vast majority of flooded agriculture, with other crops (e.g., wheat) making up a minor component of overall abundance.

Month	P1 (1988-2004)	P2 (2005-2020)	Difference	% Difference	Wilcox *p*
Jan	28,567	33,080	4,513	7%	0.683
Feb	51,834	33,785	-18,049	-21%	0.025
Mar	35,981	29,418	-6,563	-10%	0.11
Apr	15,849	18,552	2,703	8%	0.817
May	10,636	11,798	1,162	5%	0.631
Jun	4,797	6,104	1,307	12%	0.217
Jul	1,541	986	-555	-22%	0.006
Aug	565	621	56	5%	0.276
Sep	657	607	-50	-4%	0.79
Oct	910	1,689	779	30%	0.0579
Nov	5,474	6,717	1,243	10%	0.444
Dec	15,364	20,311	4,947	14%	0.276

Table S7. Central Valley all wetlands - P1 (1988-2004) and P2 (2005-20) median monthly surface water change. Areas (ha) include wetlands associated with duck clubs and wildlife refuges.

Hydroperiod	Month	P1 (1988-2004)	P2 (2004-2020)	Difference	% Difference	Wilcox *p*
	Jan	50,027	39,971	-10,055	-20%	0.009
	Feb	48,900	42,706	-6,195	-13%	0.015
	Mar	51,009	45,724	-5,285	-10%	0.041
	Apr	46,319	41,968	-4,351	-9%	0.001
	May	36,994	30,988	-6,006	-16%	0.000
semi-permanent	Jun	28,293	25,424	-2,870	-10%	0.000
	Jul	23,931	20,384	-3,548	-15%	0.000
	Aug	22,419	19,726	-2,692	-12%	0.000
	Sep	26,156	25,976	-180	-1%	0.402
	Oct	40,891	38,760	-2,131	-5%	0.127
	Nov	48,298	42,355	-5,944	-12%	0.003
	Dec	44,996	38,328	-6,668	-15%	0.008
	Jan	36,733	31,533	-5,201	-14%	0.581
	Feb	45,825	33,946	-11,879	-26%	0.136
	Mar	50,501	50,452	-48	0%	0.901
	Apr	38,922	29,354	-9,568	-25%	0.000
	May	19,058	13,085	-5,973	-31%	0.000
seasonal	Jun	8,003	5,592	-2,412	-30%	0.000
	Jul	3,727	2,149	-1,578	-42%	0.000
	Aug	2,496	1,654	-842	-34%	0.000
	Sep	4,416	4,768	352	8%	0.510
	Oct	16,910	19,477	2,567	15%	0.001
	Nov	37,080	34,713	-2,366	-6%	0.402
	Dec	42,304	41,050	-1,253	-3%	0.465
	Jan	15,661	10,588	-5,073	-32%	0.683
	Feb	20,653	9,249	-11,404	-55%	0.002
	Mar	17,209	27,987	10,779	63%	0.345
	Apr	18,074	10,163	-7,910	-44%	0.000
	May	10,296	5,896	-4,400	-43%	0.657
temporary	Jun	1,903	1,406	-498	-26%	0.204
	Jul	886	401	-485	-55%	0.002
	Aug	747	323	-424	-57%	0.001
	Sep	1,253	920	-333	-27%	0.008
	Oct	3,406	3,872	466	14%	0.817
	Nov	10,179	13,151	2,972	29%	0.094
	Dec	18,601	22,898	4,298	23%	0.557

Table S8. Central Valley wildlife refuges - P1 (1988-2004) and P2 (2005-20) median monthly surface water change. Areas (ha) exclusive to state and federally managed wildlife refuges.

Hydroperiod	Month	P1 (1988-2004)	P2 (2004-2020)	Difference	% Difference	Wilcox *p*
semi-permanent	Jan	9,005	8,562	-442	-5%	0.157
	Feb	9,370	8,602	-768	-8%	0.015
	Mar	9,445	8,961	-485	-5%	0.136
	Apr	8,987	8,312	-674	-8%	0.006
	May	5,472	4,545	-927	-17%	0.000
	Jun	3,801	3,150	-651	-17%	0.000
	Jul	3,184	2,459	-725	-23%	0.000
	Aug	2,921	2,364	-558	-19%	0.000
	Sep	5,012	4,326	-686	-14%	0.001
	Oct	7,879	7,678	-201	-3%	0.157
	Nov	8,360	8,074	-286	-3%	0.402
	Dec	7,797	7,521	-276	-4%	0.423
seasonal	Jan	6,483	6,902	419	7%	0.683
	Feb	6,830	7,086	256	4%	0.709
	Mar	7,530	8,357	827	11%	0.025
	Apr	5,158	4,866	-292	-6%	0.231
	May	2,205	1,253	-952	-43%	0.000
	Jun	1,002	482	-519	-52%	0.000
	Jul	537	231	-306	-57%	0.000
	Aug	284	156	-129	-45%	0.000
	Sep	708	630	-78	-11%	0.292
	Oct	2,840	3,257	417	15%	0.049
	Nov	3,922	5,044	1,123	29%	0.000
	Dec	3,833	5,213	1,380	36%	0.000
temporary	Jan	2,854	1,895	-959	-34%	0.041
	Feb	3,958	1,933	-2,026	-51%	0.001
	Mar	3,976	5,136	1,159	29%	0.345
	Apr	2,368	1,682	-686	-29%	0.049
	May	645	355	-289	-45%	0.000
	Jun	210	70	-140	-67%	0.000
	Jul	90	37	-53	-59%	0.000
	Aug	39	35	-4	-9%	0.326
	Sep	128	148	20	16%	0.423
	Oct	372	397	25	7%	0.901
	Nov	758	562	-196	-26%	0.345
	Dec	946	928	-18	-2%	0.763

Table S9. Central Valley duck clubs - P1 (1988-2004) and P2 (2005-20) median monthly surface water change. Areas (ha) encompass private managed wetlands on duck clubs and wildlife preserves.

Hydroperiod	Month	P1 (1988-2004)	P2 (2004-2020)	Difference	% Difference	Wilcox *p*
semi-permanent	Jan	18,106	17,435	-671	-4%	0.245
	Feb	19,614	18,062	-1,552	-8%	0.049
	Mar	19,372	18,797	-575	-3%	0.245
	Apr	17,655	16,108	-1,547	-9%	0.009
	May	13,103	11,698	-1,405	-11%	0.001
	Jun	10,305	8,883	-1,422	-14%	0.000
	Jul	7,595	6,634	-962	-13%	0.000
	Aug	6,965	6,161	-804	-12%	0.000
	Sep	8,735	8,866	131	2%	0.736
	Oct	15,700	16,090	391	2%	0.245
	Nov	17,180	16,700	-480	-3%	0.146
	Dec	16,479	15,163	-1,316	-8%	0.157
seasonal	Jan	16,563	16,604	42	>1%	0.986
	Feb	17,315	17,163	-152	-1%	0.901
	Mar	18,092	17,842	-251	-1%	0.465
	Apr	10,673	8,728	-1,945	-18%	0.000
	May	7,111	3,901	-3,210	-45%	0.000
	Jun	3,905	1,552	-2,353	-60%	0.000
	Jul	1,157	625	-532	-46%	0.000
	Aug	567	425	-142	-25%	0.004
	Sep	1,352	1,461	109	8%	0.231
	Oct	7,915	9,886	1,971	25%	0.000
	Nov	12,440	12,814	374	3%	0.094
	Dec	11,641	13,842	2,201	19%	0.037
temporary	Jan	8,283	5,199	-3,084	-37%	0.326
	Feb	8,744	4,226	-4,518	-52%	0.001
	Mar	7,702	9,929	2,228	29%	0.402
	Apr	4,124	2,816	-1,308	-32%	0.007
	May	2,431	1,351	-1,080	-44%	0.000
	Jun	962	340	-622	-65%	0.000
	Jul	269	165	-104	-39%	0.002
	Aug	145	154	8	6%	0.845
	Sep	309	242	-67	-22%	0.041
	Oct	1,200	879	-321	-27%	0.631
	Nov	2,775	2,167	-607	-22%	0.309
	Dec	6,299	3,802	-2,497	-40%	0.127

Table S10. Central Valley flooded agriculture - P1 (1988-2004) and P2 (2005-20) median monthly surface water change. Rice production accounted for the vast majority of flooded agriculture, with other crops (e.g., corn, wheat, and safflower) making up a relatively small component of overall abundance.

Month	P1 (1988-2004)	P2 (2005-2020)	Difference	% Difference	Wilcox *p*
Jan	100,562	129,178	28,616	29%	0.094
Feb	126,728	107,588	-19,140	-15%	0.168
Mar	111,633	114,714	3,081	3%	0.901
Apr	102,683	71,447	-31,235	-30%	0.000
May	187,093	200,724	13,631	7%	0.118
Jun	92,598	107,864	15,266	17%	0.053
Jul	7,764	6,685	-1,079	-14%	0.110
Aug	2,450	2,141	-308	-13%	0.069
Sep	6,306	3,716	-2,590	-41%	0.002
Oct	33,758	22,747	-11,011	-33%	0.002
Nov	62,253	109,335	47,082	76%	0.002
Dec	70,650	118,618	47,969	68%	0.001

Table S11. Major Reservoir storage in SONEC and the Central Valley (CV) - km^3 = cubic kilometers

Region	Minimum	1st Quartile	Median	Mean	3rd Quartile	Maximum
SONEC (taf)	110	455	648	654	837	1,223
CV (taf)	5,890	10,888	14,464	13,831	16,624	20,739
CV/SONEC	54	24	22	21	20	17
SONEC (km^3)	0.136	0.561	0.799	0.807	1.032	1.509
CV (km^3)	7.265	13.430	17.841	17.060	20.505	25.581

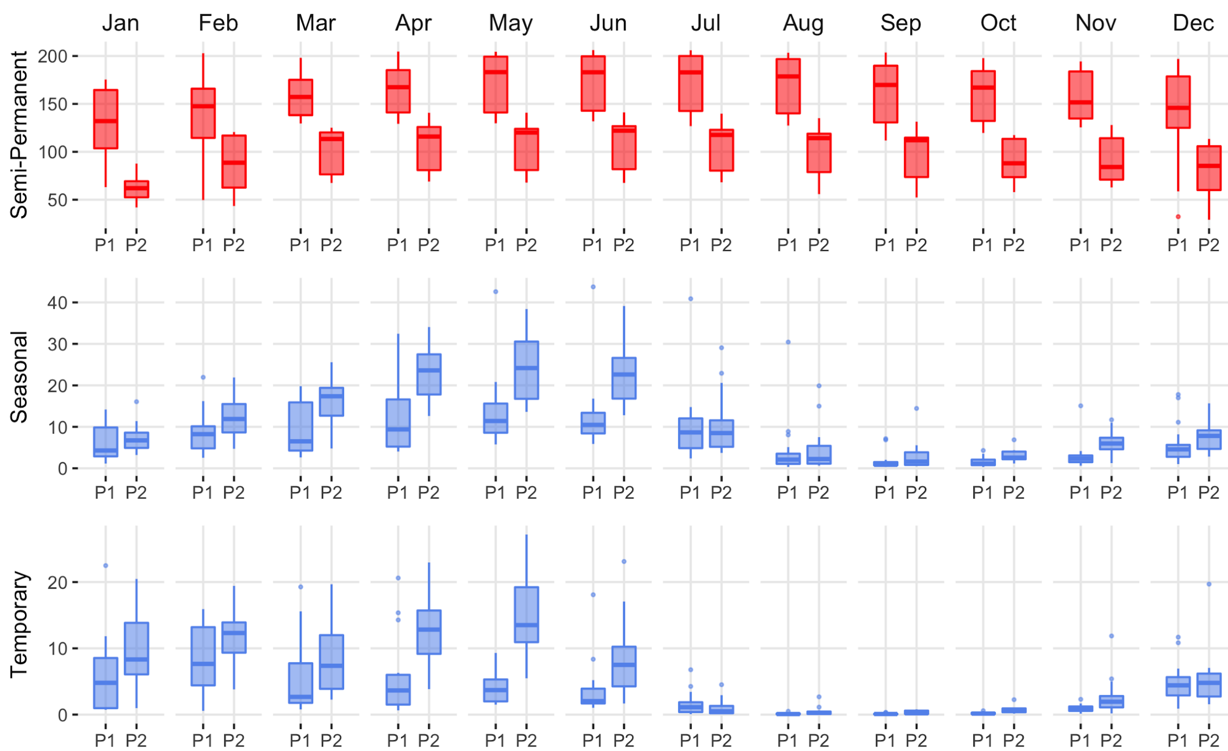

Figure S5. SONEC closed-basin lakes distribution of monthly wetland abundance (kha) between 1988-2004 (P1) and 2005-20 (P2) periods. Statistical inference determined as p-values < 0.1 derived from Wilcoxon ranked order test. Red indicates significant wetland decline and 'blue', stable to increasing wetland abundance. Results are partitioned by wetland hydroperiod (semi-permanent, seasonal, temporary). Boxes, interquartile range (IQR); line dividing the box horizontally, median value; whiskers, 1.5 times the IQR; points, outliers.

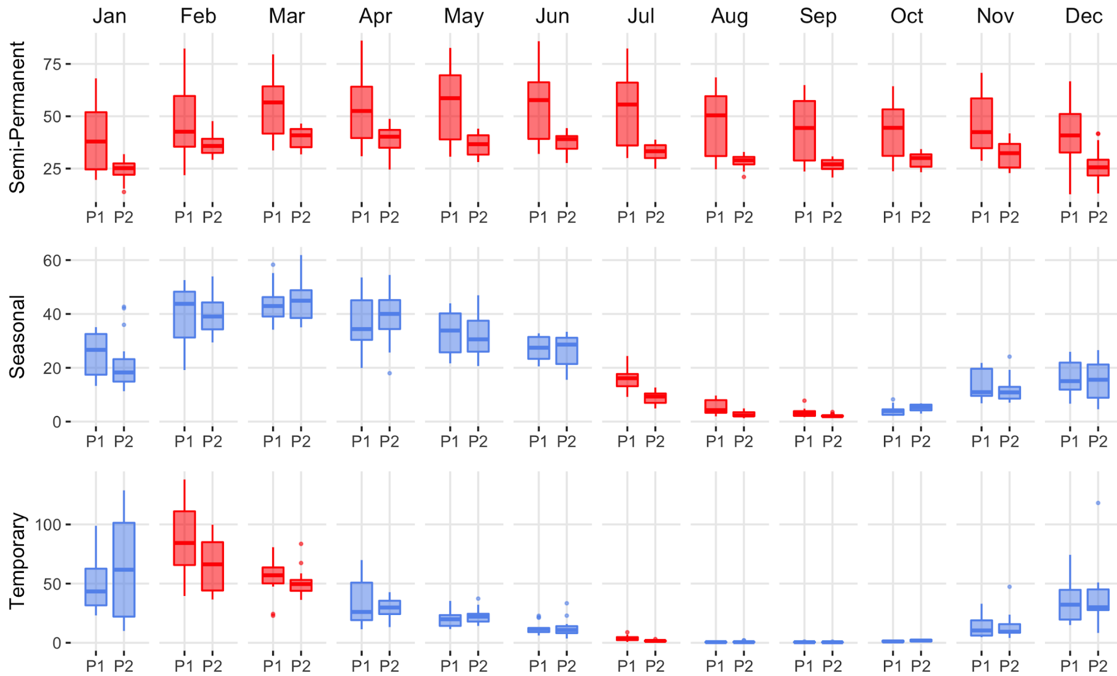

Figure S6: SONEC wildlife refuges - distribution of monthly wetland abundance (kha) from 1988-2004 (P1) and 2005-20 (P2). Areas exclusive to state and federally managed wildlife refuges. Statistical inference determined as p-values < 0.1 derived from Wilcoxon ranked order test. Red indicates significant wetland decline and 'blue', stable to expanding wetland abundance. Results are partitioned by wetland hydroperiod (semi-permanent, seasonal, temporary). Boxes, interquartile range (IQR); line dividing the box horizontally, median value; whiskers, 1.5 times the IQR; points, potential outliers.

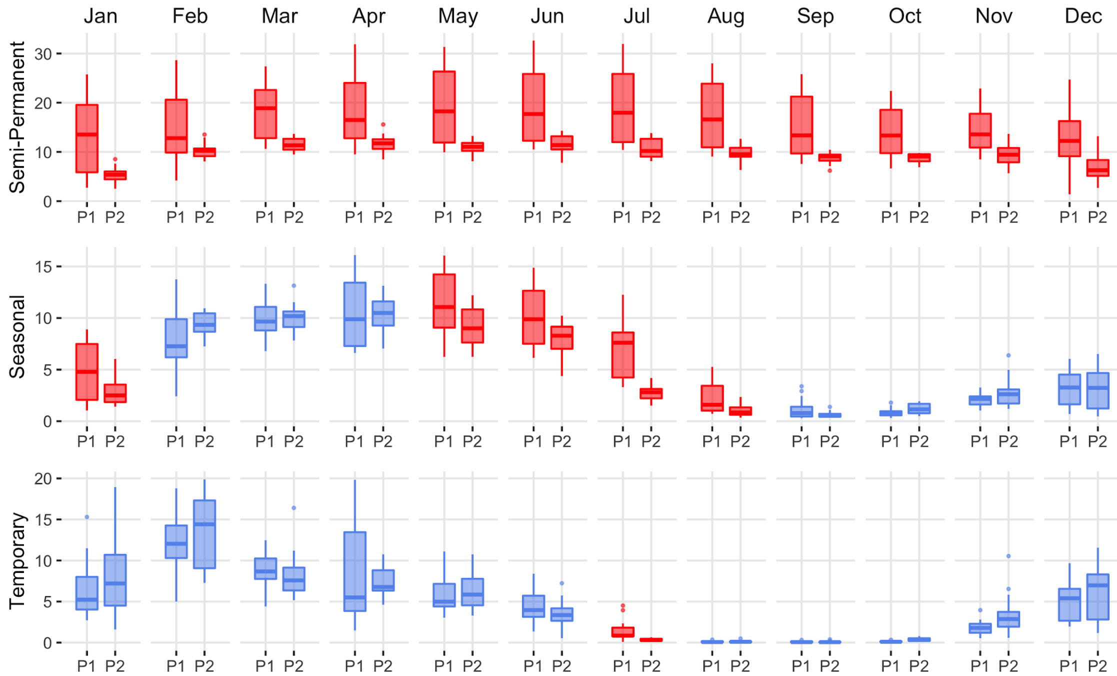

Figure S7. SONEC public wetlands - distribution of monthly wetland abundance (kha) from 1988-2004 (P1) and 2005-20 (P2) Areas include but are not limited to National Forest, Bureau of Land Management, and State Lands. Statistical inference determined as p-values < 0.1 derived from Wilcoxon ranked order test. Red indicates significant wetland decline and 'blue', stable to expanding wetland abundance. Results are partitioned by wetland hydroperiod (semi-permanent, seasonal, temporary). Boxes, interquartile range (IQR); line dividing the box horizontally, median value; whiskers, 1.5 times the IQR; points, potential outliers.

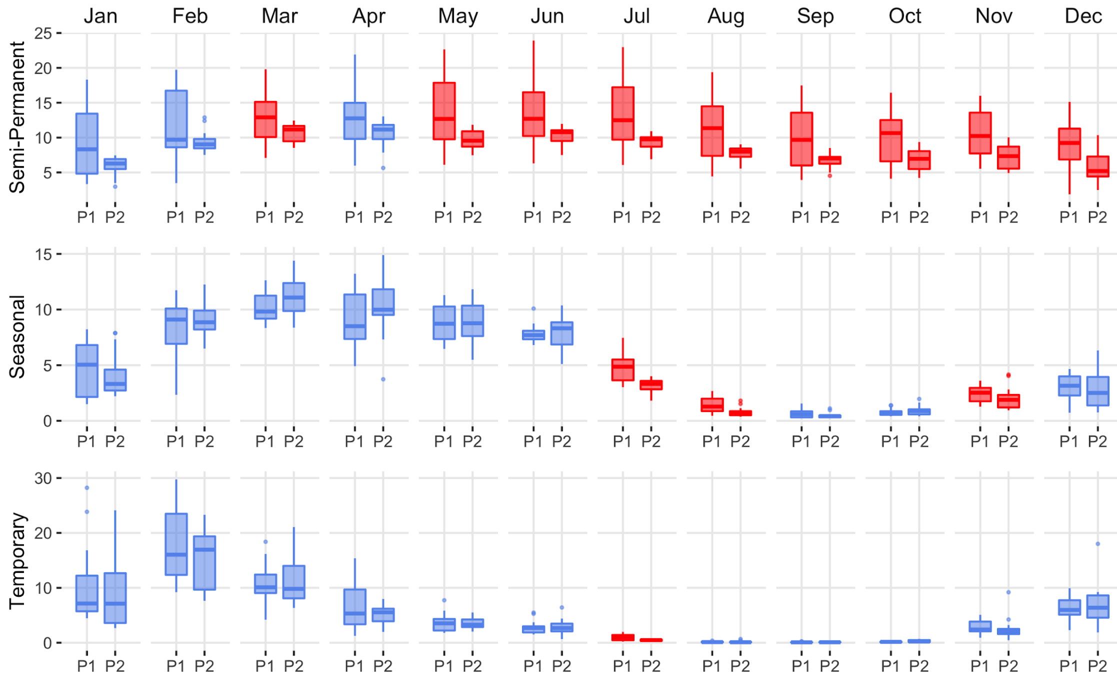

Figure S8. SONEC private wetlands - distribution of monthly wetland abundance (kha) from 1988-2004 (P1) and 2005-20 (P2). Areas were exclusive to wetlands on private lands not associated with agriculture. Statistical inference determined as p-values < 0.1 derived from Wilcoxon ranked order test. Red indicates significant wetland decline and 'blue', stable to expanding wetland abundance. Results are partitioned by wetland hydroperiod (semi-permanent, seasonal, temporary). Boxes, interquartile range (IQR); line dividing the box horizontally, median value; whiskers, 1.5 times the IQR; points, potential outliers.

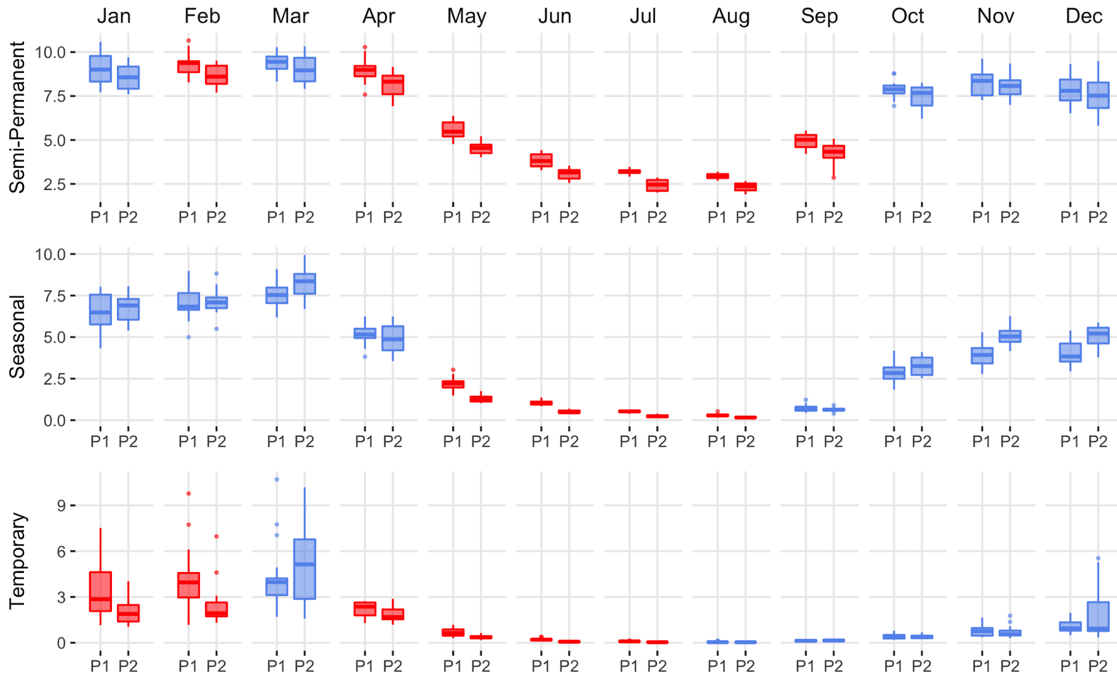

Figure S9. Central Valley wildlife refuges - distribution of monthly wetland abundance (kha) from 1988-2004 (P1) and 2005-20 (P2). Areas exclusive to state and federally managed wildlife refuges. Statistical inference determined as p-values < 0.1 derived from Wilcoxon ranked order test. Red indicates significant wetland decline and 'blue', stable to expanding wetland abundance. Results are partitioned by wetland hydroperiod (semi-permanent, seasonal, temporary). Boxes, interquartile range (IQR); line dividing the box horizontally, median value; whiskers, 1.5 times the IQR; points, potential outliers.

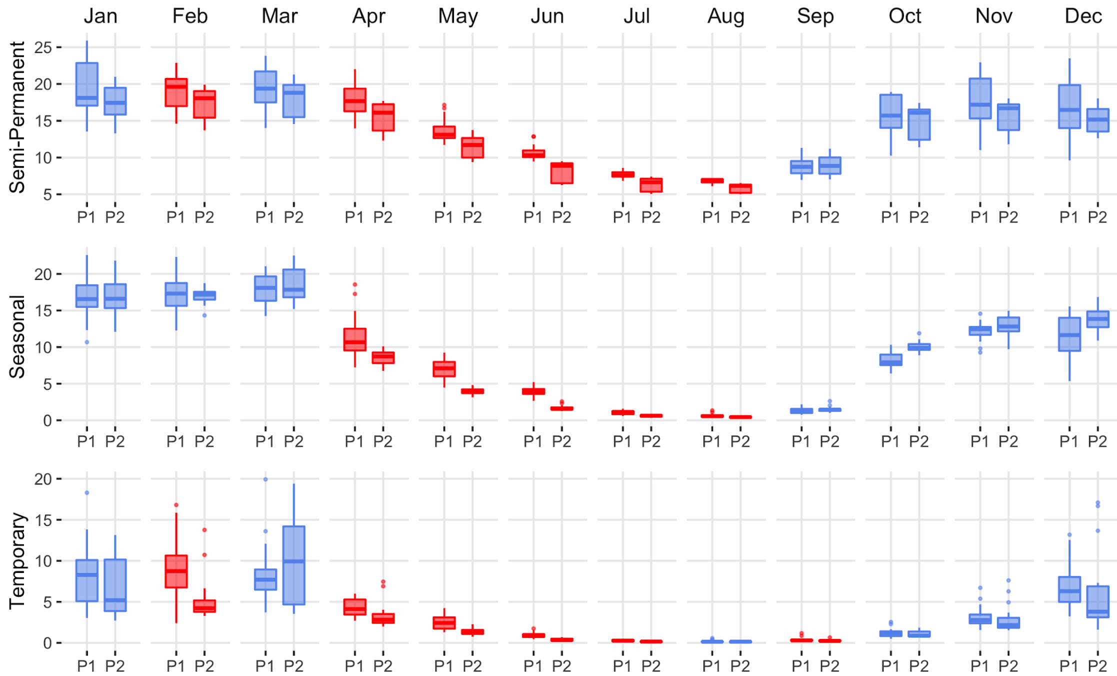

Figure S10. Central Valley duck clubs - distribution of monthly wetland abundance (kha) from 1988-2004 (P1) and 2005-20 (P2). Areas were exclusive to privately owned wetlands managed as waterfowl hunting preservers. Statistical inference determined as p-values < 0.1 derived from Wilcoxon ranked order test. Red indicates significant wetland decline and 'blue', stable to expanding wetland abundance. Results are partitioned by wetland hydroperiod (semi-permanent, seasonal, temporary). Boxes, interquartile range (IQR); line dividing the box horizontally, median value; whiskers, 1.5 times the IQR; points, potential outliers.

Supplemental Materials – Recent Climate

The regional water balance between source and use ultimately controls the surface water available for human use and wetland ecological systems in the SONEC and the Central Valley regions. The total amount of surface water is determined by precipitation, evapotranspiration, and resulting runoff, which drive groundwater recharge. These processes are highly modified by direct human factors, such as water withdrawal for industrial, domestic, and agricultural use (AghaKouchak et al., 2021). To examine climate change over the period of our analysis, we used the TerraClimate dataset (Abatzoglou et al., 2018), a gridded (4km) monthly climate and water balance model of terrestrial surfaces available through the Google Earth Engine platform (Gorelick et al., 2017). TerraClimate data is compiled using a climatically aided interpolation of relatively high resolution spatial and temporal scales, which has been validated with data from a broad climate network, including evapotranspiration and runoff, important for determining hydro-climate change (http://www.climatologylab.org/terraclimate.html). Each month was smoothed with a 5-year rolling mean to match the approach used to calculate surface water estimates to minimize inter-annual variability from exogenous and endogenous drivers. Trends were compiled using periods aligned with surface water summaries (P1=1988-2004; P2=2005-2020) and compared using nonparametric Wilcoxon rank order tests (Siegel, 1957). By comparing trends over long periods, we were able to minimize the effects of shorter-term climate cycles (e.g. El Nino Southern Oscillation; Dettinger et al., 1998) that may have influenced results. Overall results were provided as boxplots partitioned by climate variable and region. Data are presented in the following figures (Figures S11-S15) to show changes in climate variables over the periods of interest presented in the Results and Discussion sections. A p-value of < 0.1 was used to represent statistical significance.

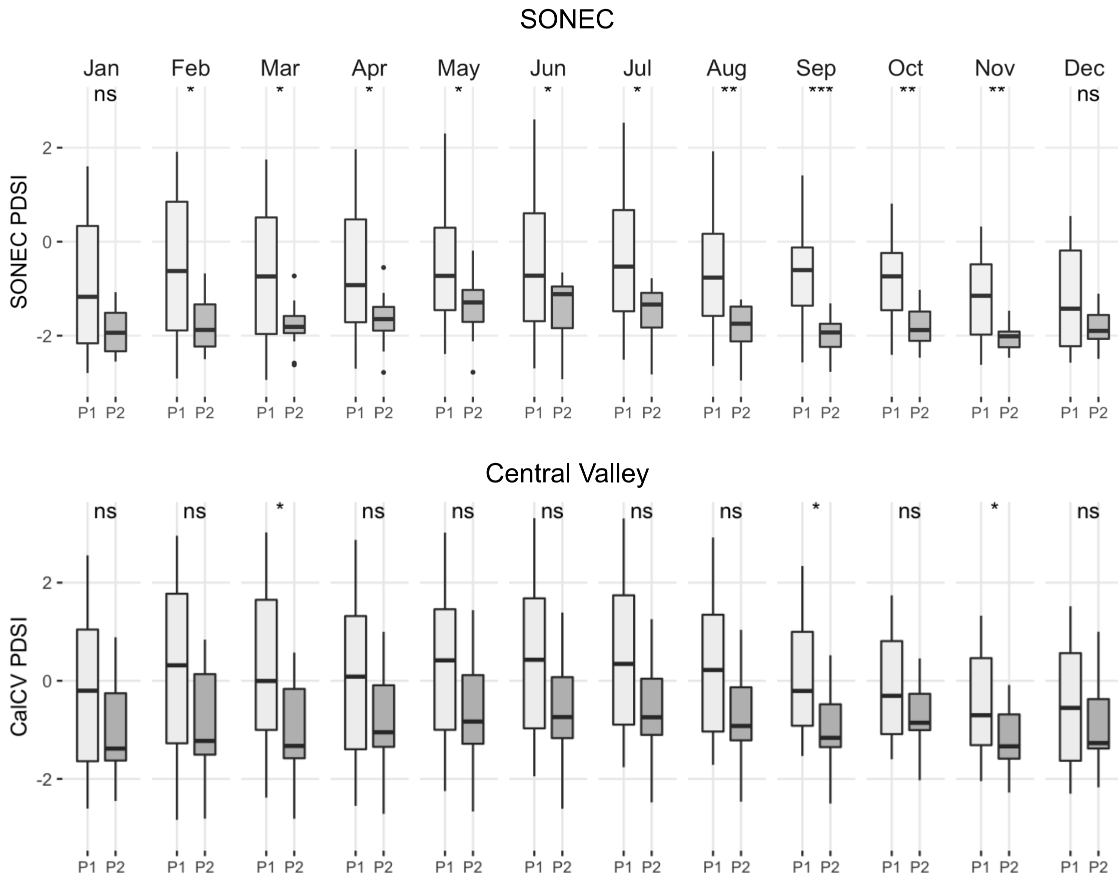

Figure S11. Distribution of monthly Palmer drought severity index (PDSI) for Southern Oregon and Northeast California (SONEC) and the Central Valley for 1988-2004 (P1) and 2005-20 (P2). Significance levels between periods are shown by symbols representing significant cut points: **** = p <0.0001, *** = p < 0.001, ** = p <0.01, * = p < 0.1, ns = non-significant. Boxes, interquartile range (IQR); line dividing the box horizontally, median value; whiskers, 1.5 times the IQR; points, potential outliers.

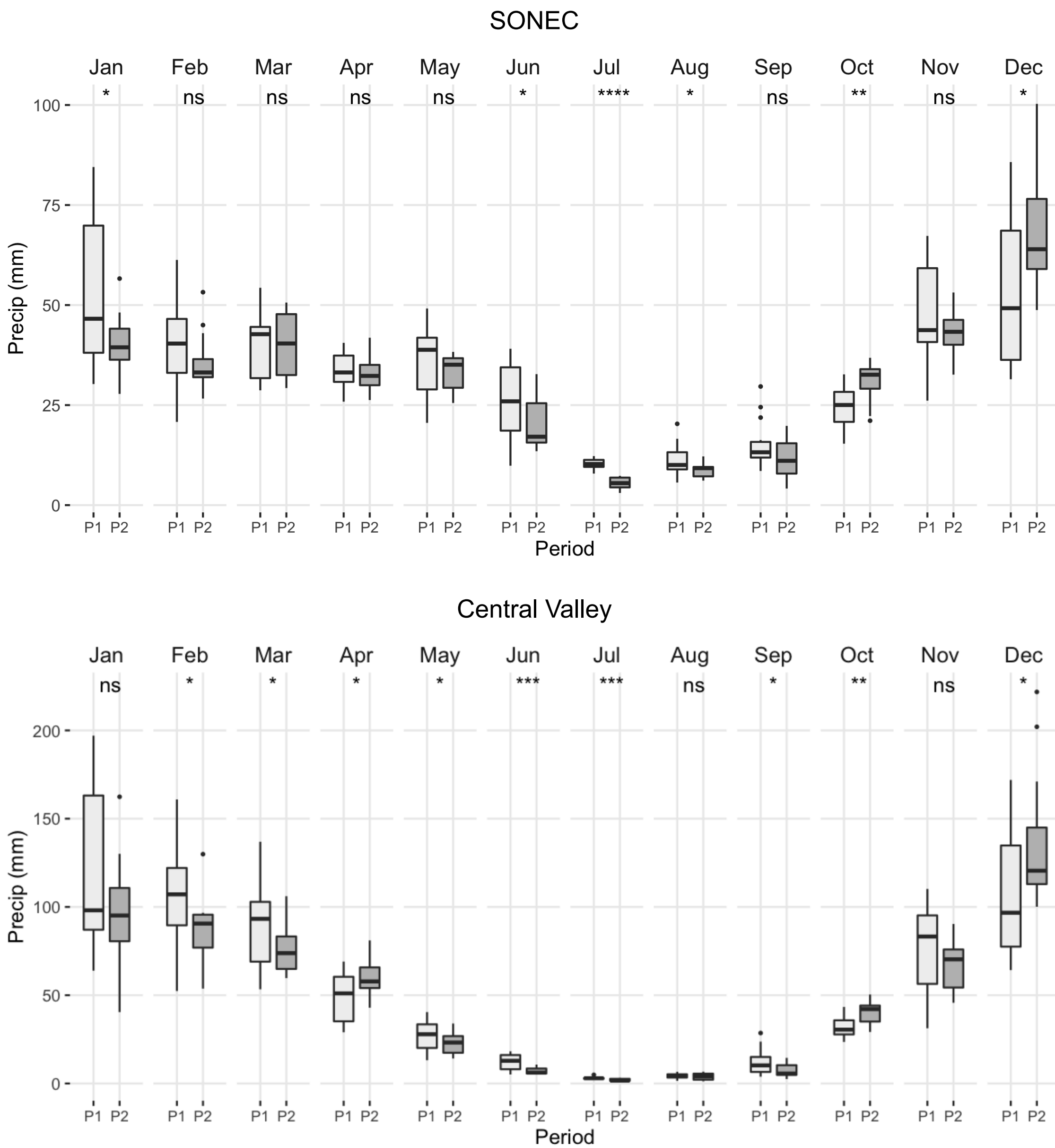

Figure S12. Distribution of monthly precipitation for Southern Oregon and Northeast California (SONEC) and the Central Valley for 1988-2004 (P1) and 2005-20 (P2). Significance levels between periods are shown by symbols representing significant cut points: **** = p <0.0001, *** = p < 0.001, ** = p <0.01, * = p < 0.1, ns = non-significant. Boxes, interquartile range (IQR); line dividing the box horizontally, median value; whiskers, 1.5 times the IQR; points, potential outliers.

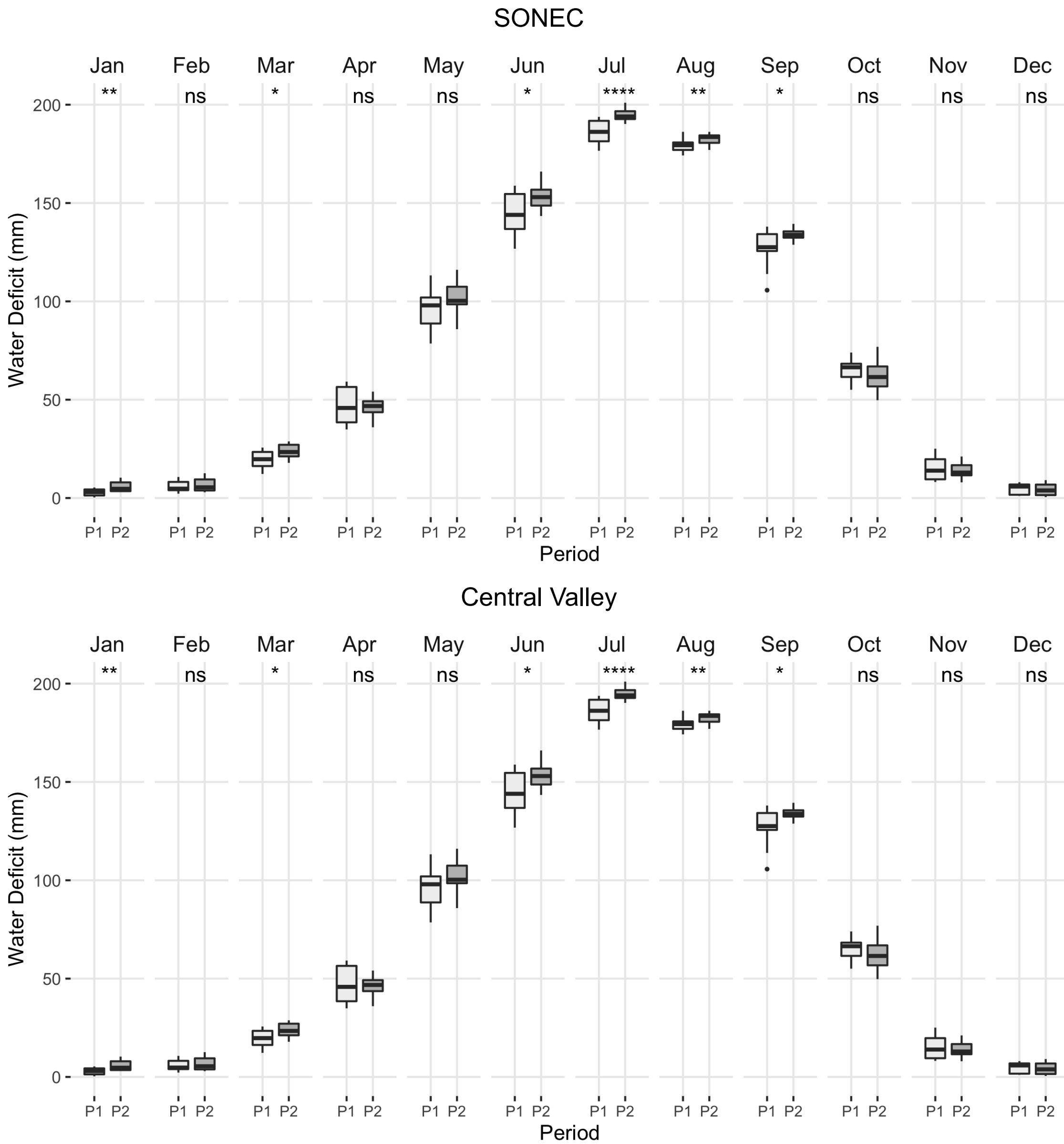

Figure S13. Distribution of monthly water deficit for Southern Oregon and Northeast California (SONEC) and the Central Valley for 1988-2004 (P1) and 2005-20 (P2). Significance levels between periods are shown by symbols representing significant cut points: **** = p <0.0001, *** = p < 0.001, ** = p <0.01, * = p < 0.1, ns = non-significant. Boxes, interquartile range (IQR); line dividing the box horizontally, median value; whiskers, 1.5 times the IQR; points, potential outliers.

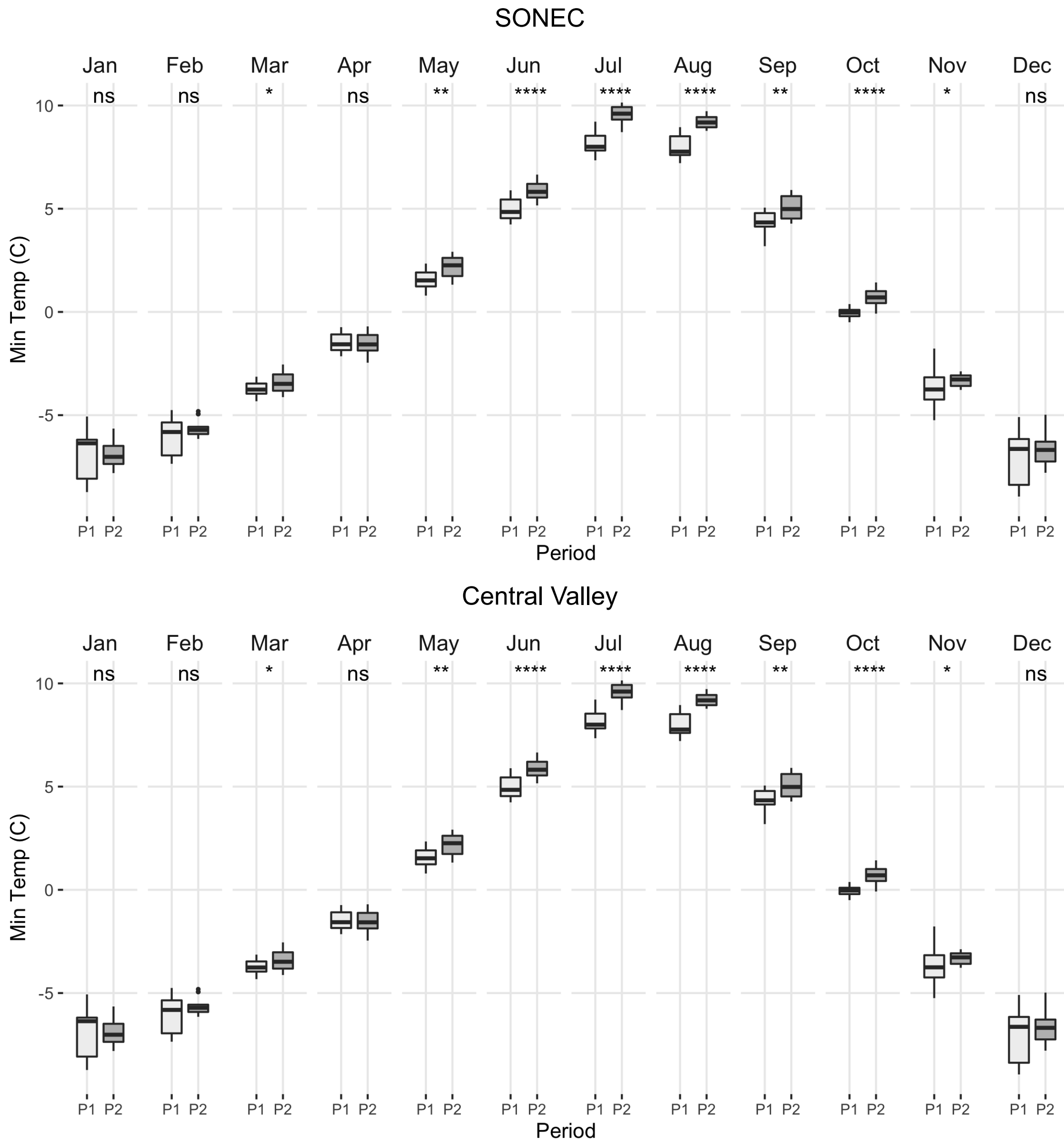

Figure S14. Distribution of monthly minimum temperatures for Southern Oregon and Northeast California (SONEC) and the Central Valley for 1988-2004 (P1) and 2005-20 (P2). Significance levels between periods are shown by symbols representing significant cut points: **** = p <0.0001, *** = p < 0.001, ** = p <0.01, * = p < 0.1, ns = non-significant. Boxes, interquartile range (IQR); line dividing the box horizontally, median value; whiskers, 1.5 times the IQR; points, potential outliers.

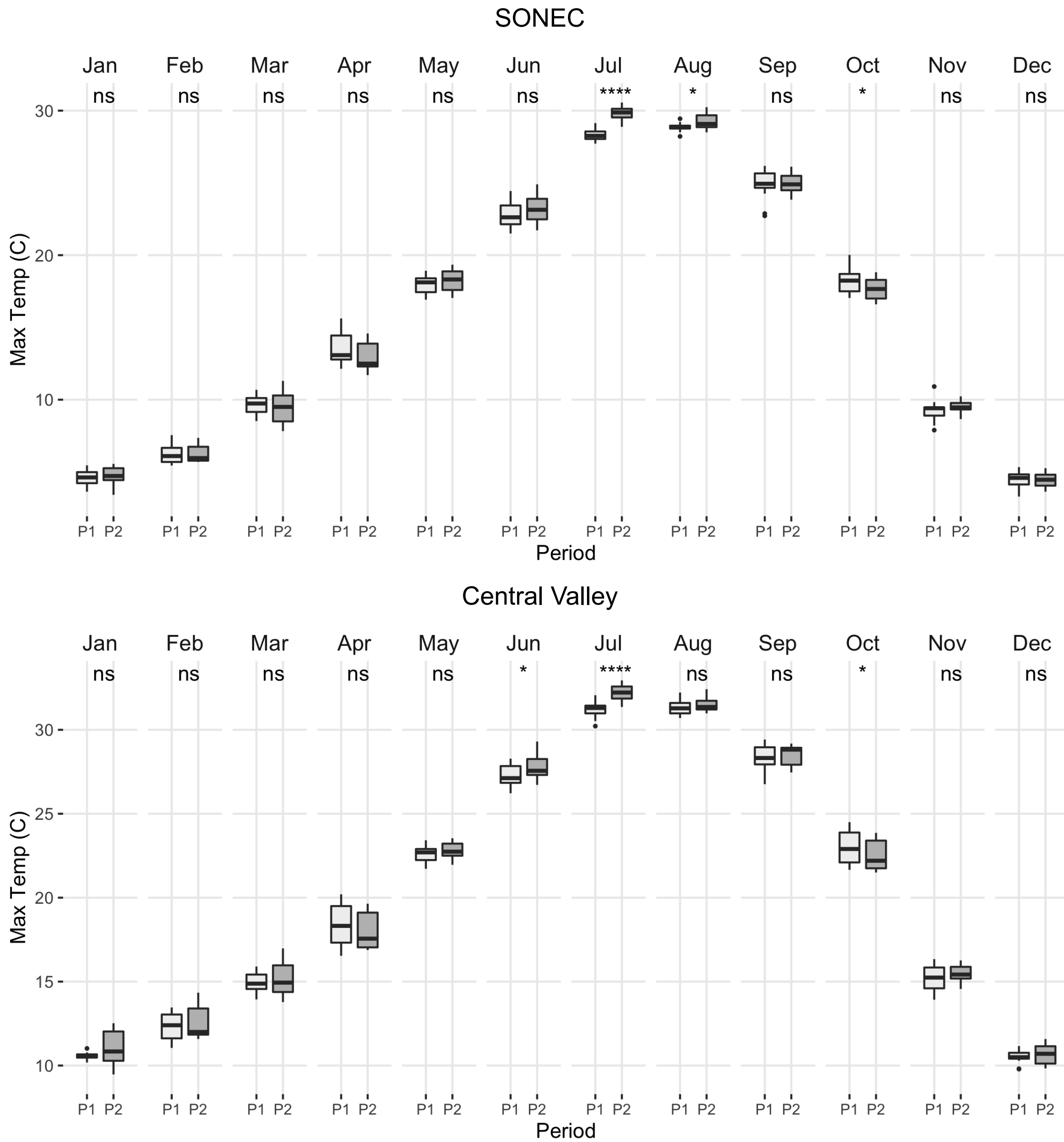

Figure S15. Distribution of monthly maximum temperatures for Southern Oregon and Northeast California (SONEC) and the Central Valley for 1988-2004 (P1) and 2005-20 (P2). Significance levels between periods are shown by symbols representing significant cut points: **** = p <0.0001, *** = p < 0.001, ** = p <0.01, * = p < 0.1, ns = non-significant. Boxes, interquartile range (IQR); line dividing the box horizontally, median value; whiskers, 1.5 times the IQR; points, potential outliers.

Supplemental Materials – Future Climate

To examine the potential future climate of the SONEC and the Central Valley regions, we used the MACAv2-METDATA Monthly Summaries accessed in the Google Earth Engine Platform. The dataset is statistically downscaled from global climate model output from the Coupled Model Intercomparison Project 5 (CMIP5, Taylor et al. 2010) utilizing a modification of the Multivariate Adaptive Constructed Analogs (MACA) approach (Abatzoglou and Brown, 2012) with the “Livneh" observational dataset as training data (Livneh et al., 2013). MACAAv2 has a 4-km grid-scale for historical (1950-2005) and future (2006-2100) climate metrics (maximum and minimum temperature, humidity, precipitation, and downward shortwave radiation), compiled for 20 global climate models. Detailed information on methods and available data can be found at the MACA homepage (https://climate.northwestknowledge.net/MACA/index.php).

We used an ensemble of downscaled climate models to estimate variability in future climate outcomes (Mote et al., 2011). To access both model and scenario uncertainty (Hawkins and Sutton, 2009) we compiled data from a set of models run under two future representative concentration pathways (RCP) RCP 4.5 and RCP 8.5. RCP 4.5, an intermediate scenario, has CO_2-equivalent emissions peaking ~2040, then declining through 2100 (Fig. 2 in Meinshausen, et al. 2011; https://ar5-syr.ipcc.ch/topic_futurechanges.php, Box 2.2, Figure. 1). RCP 8.5 assumes emissions steadily rise through 2100 and, although "increasingly implausible with each passing year" (Hausfather and Peters, 2020), represents a high-emission boundary condition or “worst-case” climate change scenario (*ibid*). RCP 8.5 and RCP4.5 temperature projections are approximately consistent with the model outcomes from the 2000 Special Report on Emission Scenarios, respectively (Hayhoe et al., 2017), representing the potential global maximum temperature response (~ 4-10°C by 2100) and a more moderate response ~ 2-4°C by 2100).

Although some studies suggest that projections from a random set of climate models are similar to those of the “best” models based on comparison to historical data, we used results from Rupp et al. (2013) to inform model selection rather than using all 20 MACAv2 models. Rupp et al. (2013) found that for the Pacific Northwest region (which overlaps most of the SONEC and the Central Valley regions), there was a significant difference among 41 downscaled climate models. However, a clear set of models did a better job of reproducing historical conditions over 18 climate metrics. This was especially true for the metrics measuring the seasonal amplitude and inter-annual/seasonal variability of precipitation and temperature, metrics important for understanding wetland response to climate and waterbird use of wetland systems. Therefore we decided to use the models that overlapped between the top-20 models of Rupp et al. and those available in MACAAv2. This resulted in a set of 7 models (Table S12).

Table S12. List of models used from the MACAv2 GEE dataset that are in the “best” performing models (top ~15) of Rupp, et al. (2013).

MODEL	**SOURCE AGENCY**
CanESM2	Canadian Center for Climate Modeling and Analysis
CCSM4	National Center of Atmospheric Research, USA
HadGEM2-CC	Met Office Hadley Center, UK
HadGEM2-ES	Met Office Hadley Center, UK
IPSL-CM5B-MR	Institute Pierre Simon Laplace, France
MICROC5	Japan (three institutes)
NorESM1-M	Norwegian Climate Center, Norway

Although this is a relatively small number of models for ensemble analysis (https://climate.northwestknowledge.net/MACA/GCMselection.php), we chose this approach because of the lower relative error of variables of interest in this set of MACAv2-available model outcomes provides a stronger gage of variability/uncertainty of future climate projections in the SONEC-Central Valley regions.

We extracted MACAv2 values from these seven models for the RCP 4.5 and RCP 8.5 scenarios to determine precipitation and temperature (maximum and minimum) for each water year from the historical period from 1950-1999 and the future from 2039-2099 (three ~ 20-year periods). Rather than using modeled actual values, we calculated and plotted future anomalies for temperature and precipitation based on the 1950-1999 period median values (see following Figures S16-17). The changes in three climate variables, minimum temperature (TMIN), maximum temperature (TMAX), and precipitation (PR) in the future from this assemblage of models are presented. In all cases, anomalies are plotted based on the historical 1950-1999 period.

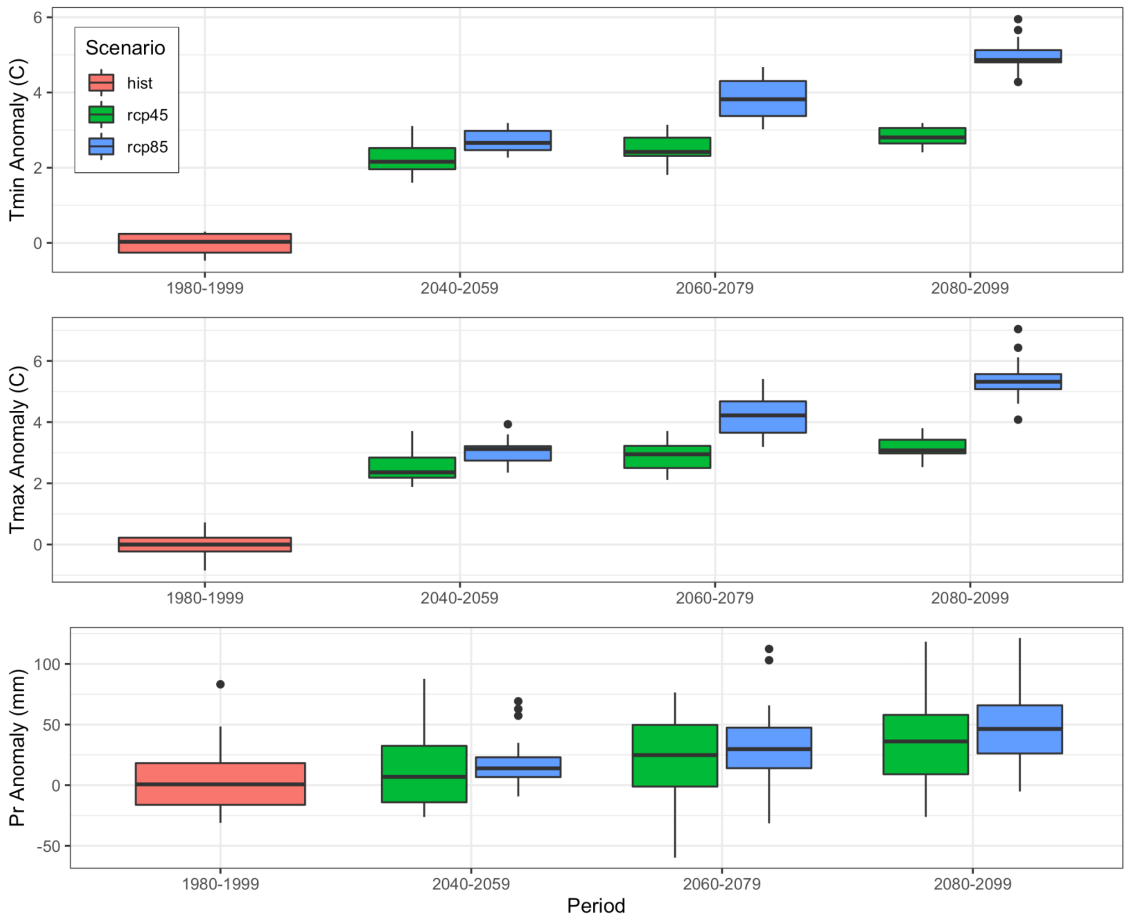

Figure S16. Future Southern Oregon and Northeast California (SONEC) climate projections for historic, RCP 4.5, and RCP 8.5 emission scenarios. Estimates were derived from an ensemble of seven downscaled climate models extracted from the MACAv2 dataset.

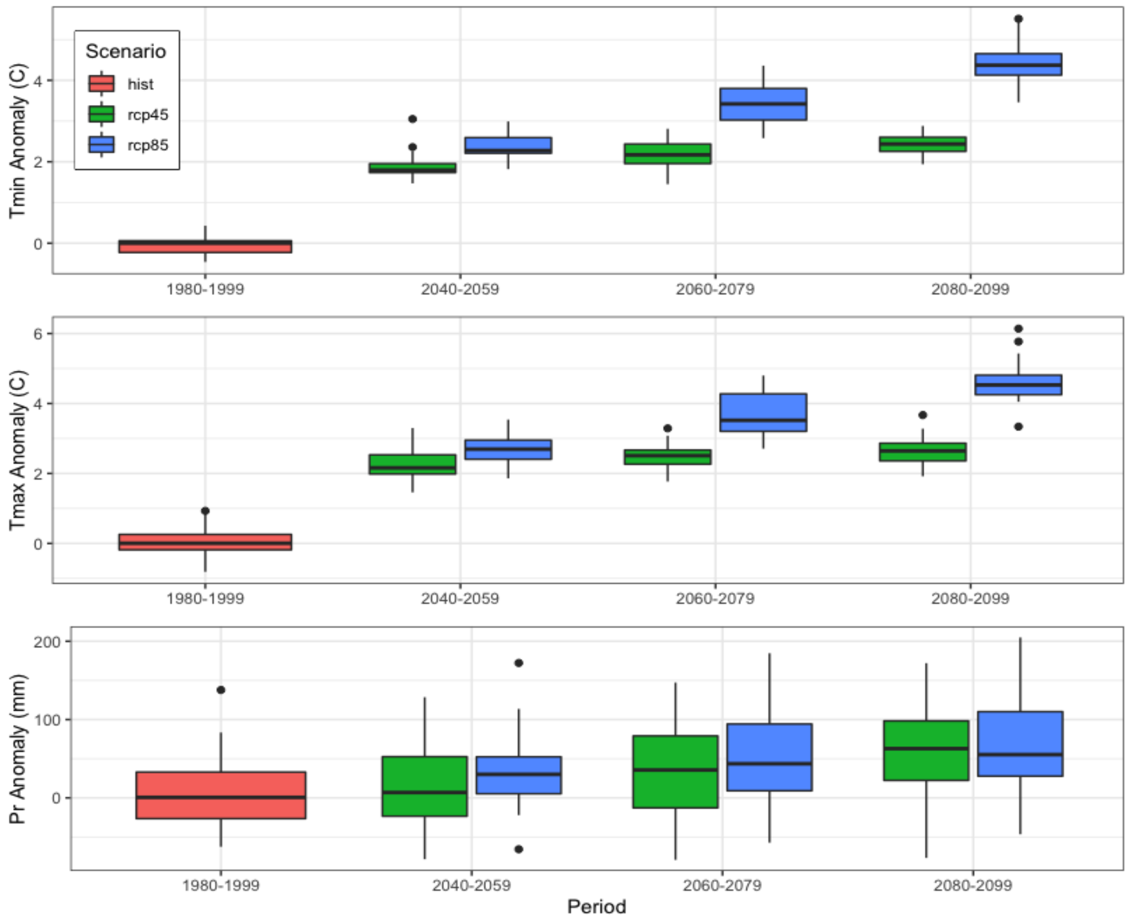

Figure S17. Future Central Valley climate projections for historic, RCP 4.5, and RCP 8.5 emission scenarios. Estimates were derived from an ensemble of seven downscaled climate models extracted from the MACAv2 dataset.

We calculated a time series of the Standardized Precipitation Evapotranspiration Index (SPEI) using MACAv2 values (Vicente-Serrano et al., 2014). The SPEI considers precipitation (PRCP) and potential evapotranspiration (PET) in estimating drought, capturing the impact of temperature on water demand. The SPEI also correlates well with the self-calibrating Palmer Drought Severity Index (scPDS I) at 1-18 month timescales, the scale at which we examine changing wetland surface areas. To estimate potential drought in the future, we used MACAv2 data as input to the R-package SPEI (Vicente-Serrano et al., 2010). We calculated PET by the Hargreaves method (Hargreaves and Samani, 1985) and then calculated the SPEI time series from 1950 to 2100, the time range of the MACAv2 data. We used the period just before our surface water analysis, 1950-1985, as the reference period. SPEI was then calculated for the complete time series using “historical”, “RCP45”, and “RCP85” scenarios in the MACAv2 data for each region, SONEC, and the Central Valley. This resulted in four time series representing potential future drought under an intermediate CO_2-equivalent emissions scenario (RCP 4.5) and a high-emission change scenario (RCP 8.5, Figures S18 & S19.

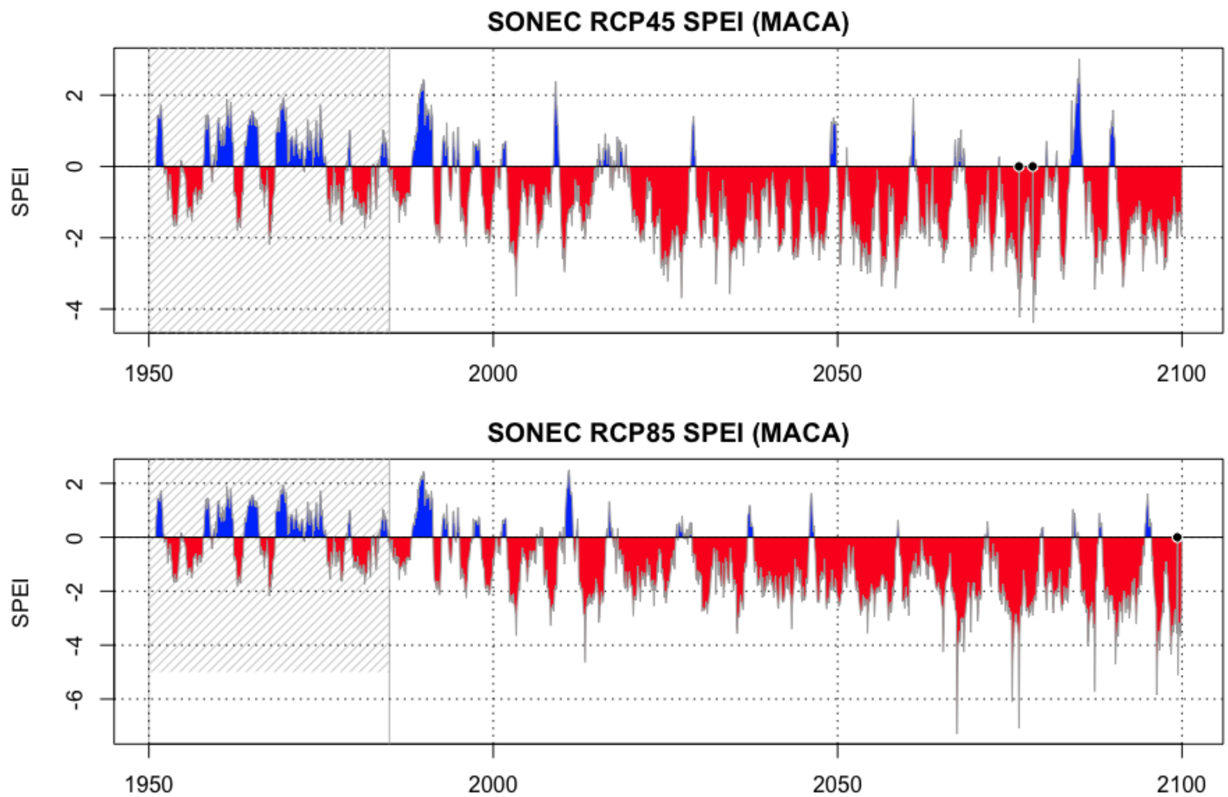

Figure S18. Southern Oregon and Northeast California (SONEC) Standardized Precipitation Evapotranspiration Index (SPEI) from 1950-2100 for RCP 4.5, and RCP 8.5 emissions scenarios. Predictions derived using a modification of the Multivariate Adaptive Constructed Analogs approach (MACA). Reference period is shaded, 1950 -1985.

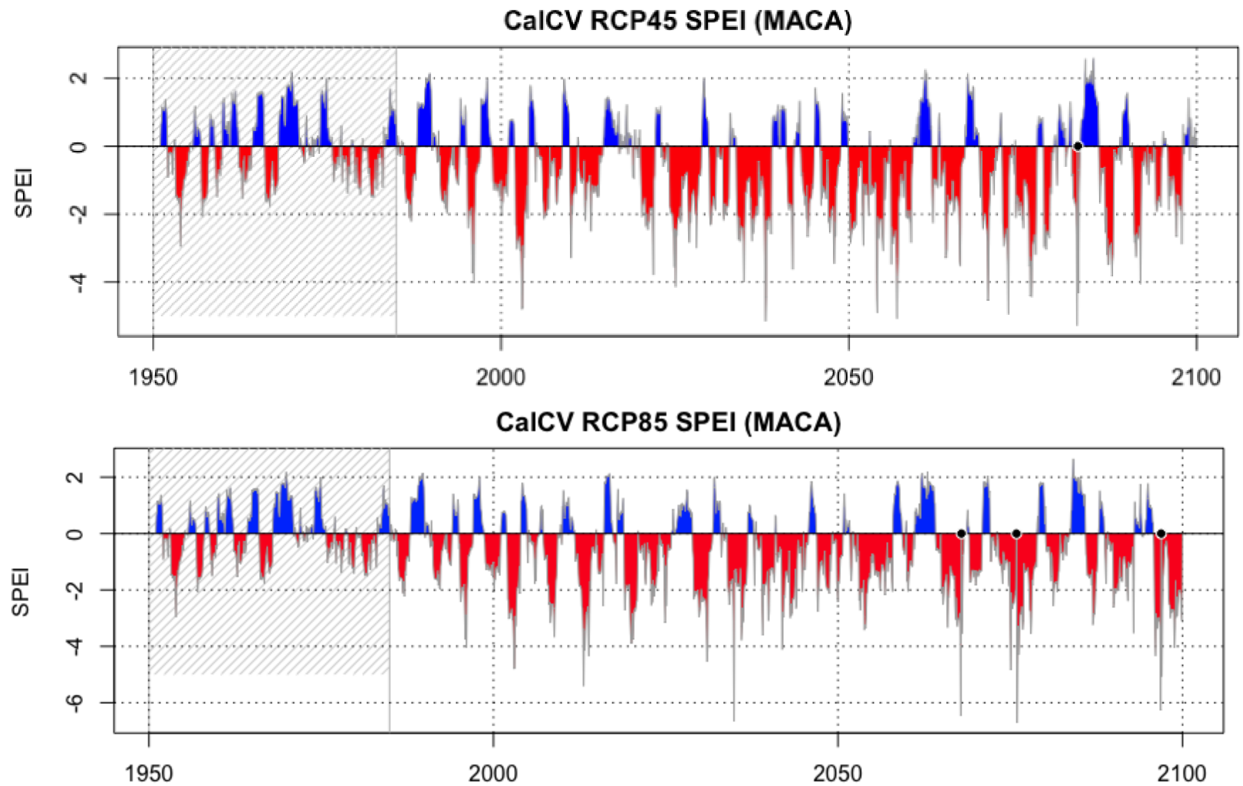

Figure S19. Central Valley (CalCV) standardized precipitation evapotranspiration index (SPEI) from 1950-2100 for RCP 4.5, and RCP 8.5 emissions scenarios. Predictions derived using a modification of the Multivariate Adaptive Constructed Analogs approach (MACA). Reference period is shaded, 1950 -1985.

References

Abatzoglou, J. T., and Brown, T. J. (2012). A comparison of statistical downscaling methods suited for wildfire applications. *Int. J. Climatol.* 32, 772–780. doi:10.1002/joc.2312.

Abatzoglou, J. T., Dobrowski, S. Z., Parks, S. A., and Hegewisch, K. C. (2018). TerraClimate, a high-resolution global dataset of monthly climate and climatic water balance from 1958–2015. *Scientific Data* 5, 170191. doi:10.1038/sdata.2017.191.

Adams, J. B., and Gillespie, A. R. (2006). *Remote Sensing of Landscapes with Spectral Images: A Physical Modeling Approach*. Cambridge University Press Available at: https://play.google.com/store/books/details?id=v8jLCgAAQBAJ.

AghaKouchak, A., Mirchi, A., Madani, K., Di Baldassarre, G., Nazemi, A., Alborzi, A., et al. (2021). Anthropogenic drought: Definition, challenges, and opportunities. *Rev. Geophys.* 59. doi:10.1029/2019rg000683.

Box, E. O., Holben, B. N., and Kalb, V. (1989). Accuracy of the AVHRR vegetation index as a predictor of biomass, primary productivity and net CO2 flux. *Vegetatio* 80, 71–89. doi:10.1007/BF00048034.

Callaghan, C. T., and Gawlik, D. E. (2015). Efficacy of eBird data as an aid in conservation planning and monitoring. *J. Field Ornithol.* 86, 298–304. doi:10.1111/jofo.12121.

Dettinger, M. D., Cayan, D. R., Diaz, H. F., and Meko, D. M. (1998). North–South Precipitation Patterns in Western North America on Interannual-to-Decadal Timescales. *J. Clim.* 11, 3095–3111. doi:10.1175/1520-0442(1998)011<3095:NSPPIW>2.0.CO;2.

DeVries, B., Huang, C., Lang, M. W., Jones, J. W., Huang, W., Creed, I. F., et al. (2017). Automated Quantification of Surface Water Inundation in Wetlands Using Optical Satellite Imagery. *Remote Sensing* 9, 807. doi:10.3390/rs9080807.

Donnelly, J. P., King, S. L., Knetter, J., Gammonley, J. H., Dreitz, V. J., Grisham, B. A., et al. (2021). Migration efficiency sustains connectivity across agroecological networks supporting sandhill crane migration. *Ecosphere* 12. doi:10.1002/ecs2.3543.

Donnelly, J. P., Naugle, D. E., Collins, D. P., Dugger, B. D., Allred, B. W., Tack, J. D., et al. (2019). Synchronizing conservation to seasonal wetland hydrology and waterbird migration in semi‐arid landscapes. *Ecosphere* 10, 1–12. doi:10.1002/ecs2.2758.

Foga, S., Scaramuzza, P. L., Guo, S., Zhu, Z., Dilley, R. D., Beckmann, T., et al. (2017). Cloud detection algorithm comparison and validation for operational Landsat data products. *Remote Sens. Environ.* 194, 379–390. doi:10.1016/j.rse.2017.03.026.

Gorelick, N., Hancher, M., Dixon, M., Ilyushchenko, S., Thau, D., and Moore, R. (2017). Google Earth Engine: Planetary-scale geospatial analysis for everyone. *Remote Sens. Environ.* 202, 18–27. doi:10.1016/j.rse.2017.06.031.

Halabisky, M., Moskal, L. M., Gillespie, A., and Hannam, M. (2016). Reconstructing semi-arid wetland surface water dynamics through spectral mixture analysis of a time series of Landsat satellite images (1984–2011). *Remote Sens. Environ.* 177, 171–183. doi:10.1016/j.rse.2016.02.040.

Hargreaves, G. H., and Samani, Z. A. (1985). Reference crop evapotranspiration from temperature. *Appl. Eng. Agric.* 1, 96–99. doi:10.13031/2013.26773.

Hausfather, Z., and Peters, G. P. (2020). Emissions – the "business as usual" story is misleading. *Nature* 577, 618–620. doi:10.1038/d41586-020-00177-3.

Hawkins, E., and Sutton, R. (2009). The Potential to Narrow Uncertainty in Regional Climate Predictions. *Bull. Am. Meteorol. Soc.* 90, 1095–1108. doi:10.1175/2009BAMS2607.1.

Hayhoe, K., Edmonds, J., Kopp, R., LeGrande, A., Sanderson, B., Wehner, M., et al. (2017). Climate models, scenarios, and projections. Available at: https://digitalcommons.unl.edu/usdeptcommercepub/589/ [Accessed February 13, 2022].

Jin, Huiran Huang, Chengquan Lang, Megan W Yeo, In-Young Stehman, Stephen V (2017). Monitoring of wetland inundation dynamics in the Delmarva Peninsula using Landsat time-series imagery from 1985 to 2011. *Remote Sens. Environ.* 190, 26–41. doi:10.1016/j.rse.2016.12.001.

Jolly, I. D., McEwan, K. L., and Holland, K. L. (2008). A review of groundwater–surface water interactions in arid/semi‐arid wetlands and the consequences of salinity for wetland ecology. *Ecohydrol.* 1, 43–58. Available at: http://onlinelibrary.wiley.com/doi/10.1002/eco.6/full.

Livneh, B., Rosenberg, E. A., Lin, C., Nijssen, B., Mishra, V., Andreadis, K. M., et al. (2013). A Long-Term Hydrologically Based Dataset of Land Surface Fluxes and States for the Conterminous United States: Update and Extensions. *J. Clim.* 26, 9384–9392. doi:10.1175/JCLI-D-12-00508.1.

McFeeters, S. K. (1996). The use of the Normalized Difference Water Index (NDWI) in the delineation of open water features. *Int. J. Remote Sens.* 17, 1425–1432. doi:10.1080/01431169608948714.

Mote, P., Brekke, L., Duffy, P. B., and Maurer, E. (2011). Guidelines for constructing climate scenarios. *Eos* 92, 257–258. doi:10.1029/2011eo310001.

QGIS Development Team (2020). *QGIS*. Open Source Geospatial Foundation Project Available at: http://qgis.osgeo.org.

Rupp, D. E., Abatzoglou, J. T., Hegewisch, K. C., and Mote, P. W. (2013). Evaluation of CMIP5 20thcentury climate simulations for the pacific northwest USA. *J. Geophys. Res.* 118, 10,884–10,906. doi:10.1002/jgrd.50843.

Siegel, S. (1957). Nonparametric Statistics. *Am. Stat.* 11, 13–19. doi:10.1080/00031305.1957.10501091.

Sullivan, B. L., Wood, C. L., Iliff, M. J., Bonney, R. E., Fink, D., and Kelling, S. (2009). eBird:

A citizen-based bird observation network in the biological sciences. *Biol. Conserv.* 142, 2282–2292. doi:10.1016/j.biocon.2009.05.006.

Vicente-Serrano, S. M., Beguería, S., and López-Moreno, J. I. (2010). A Multiscalar Drought Index Sensitive to Global Warming: The Standardized Precipitation Evapotranspiration Index. *J. Clim.* 23, 1696–1718. doi:10.1175/2009JCLI2909.1.

Vicente-Serrano, S. M., Sergio, M., and Others (2014). The climate data guide: Standardized precipitation evapotranspiration index (SPEI).

Walker, J., and Taylor, P. D. (2017). Using eBird data to model population change of migratory bird species. *Avian Conserv. Ecol./Ecol. Conserv. Oiseaux* 12. doi:10.5751/ace-00960-120104.